Unveiling 3D Biological Structures by X-ray Microtomography

R. Mizutani[1]*, A. Takeuchi[2], K. Uesugi[2], S. Takekoshi[3], R.Y. Osamura[3], and Y. Suzuki[2]

[1] Department of Applied Biochemistry, School of Engineering, Tokai University, Kanagawa 259-1292, Japan
[2] Research and Utilization Division, JASRI/SPring-8, Hyogo 679-5198, Japan
[3] Department of Pathology, Tokai University School of Medicine, Kanagawa 259-1193, Japan
* To whom correspondence should be addressed (ryuta@tokai-u.jp).

In this paper, we provide an introduction to the microtomographic analysis of three-dimensional (3D) biological structures such as neuronal circuits, which are built up by neurons as a 3D network. Unveiling the 3D biological structures is the first step to understanding the mechanism of biological functions. A practical basis for spatial resolution, viewing field, and exposure time are outlined. Contrast enhancement with high-Z probe elements is described and the observation wavelength is considered. Structural analyses of human and mouse brain networks are presented as examples of application to 3D biological structure visualization. A methodology for building skeletonized wire models in 3D coefficient maps is illustrated by analogy to a method used in macromolecular crystallography. Our results indicate that x-ray microtomography is a potential method of unveiling 3D microstructures relevant to biological functions, like x-ray crystallography in molecular biology.

Keywords micro-CT; synchrotron radiation; cerebral cortex

1. Why microtomography?

How can we determine three-dimensional (3D) biological structures? Some people might say that we can visualize 3D objects by using electron microscopy. An example of such a micrograph is shown in Figure 1a. We can see micrometer-sized rectangular wells carved on an aluminum wire, as if we had visualized the 3D structure. However, this is only a two-dimensional (2D) picture. We cannot see how deep the wells are or what the sample's inner structures are. Information about the 3D structure is not included in this micrograph because this picture only represents the appearance of the sample surface owing to the low permeability of the electron or ion beam used in this method. Therefore, 3D visualization of a sample with a biologically relevant thickness is difficult.

Others might say that we usually visualize 3D structures of biological samples by using light microscopy. Indeed, biological structures specifically labeled with fluorescent probes can be visualized with fluorescence confocal microscopy [1]. A 3D image can be created by stacking 2D micrographs. However, the absorptive and refractile nature of biological tissue for ultraviolet, visible, and infrared light makes it difficult to visualize 3D microstructures existing deep in block samples. This actually results in anisotropy among the image dimensions. While the number of pixels in the micrograph plane is over 1000 x 1000, the number along the direction perpendicular to the micrograph plane is typically 100 at most.

In contrast, the transmissive and less refractile nature of x-rays with respect to biological tissue enables radiographic observation of inner structures. X-ray computed tomography (CT) is one such radiographic technique and it is used for visualizing 3D structures. Because the wavelength of hard x-rays is several thousand times shorter than that of the visible light used in light microscopy, the diffraction-limited resolution of x-ray microscopy is much higher than that of light microscopy. The application of x-ray microscopic approaches to CT analysis [2-4] has led to the visualization of 3D microstructures. The example of microtomographic analysis in Figure 1b reveals the 3D microstructures of the rectangular well patterns. This figure clearly indicates that x-ray microtomography (micro-CT) can visualize not only the surface appearance but the 3D density distribution.

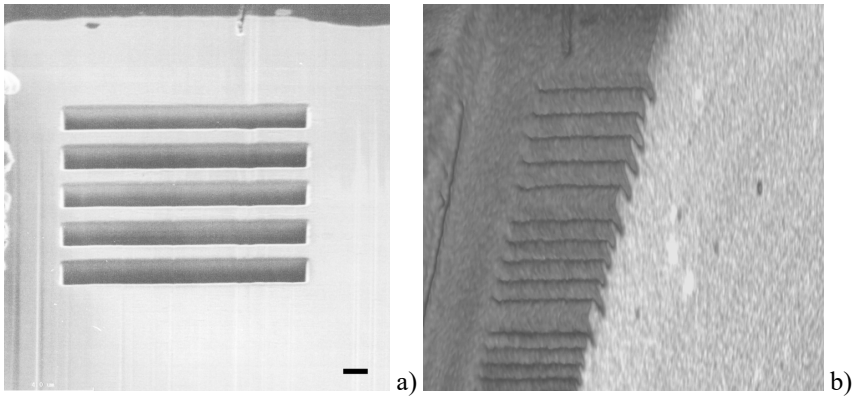

Fig. 1 Visualization of rectangular wells carved on an aluminum surface. (a) Secondary electron image of 2.0-μm pitch wells taken with a focused ion-beam apparatus. Only the surface was visualized. Scale bar: 1 μm. This figure is reprinted from ref. 13 with permission from Elsevier. (b) Microtomographic 3D image of similar patterns with pitches of 2.0 μm, 1.6 μm and 1.2 μm taken using zone plate optics. The right side end of the sample was cut off to reveal the cross section. The pattern profiles along with internal structures were visualized.

2. Microtomography in practice

2.1 Sample preparation

Microtomographic analysis is performed by recording 2D radiographs of a sample by rotating the sample itself. The acquired images are then subjected to the tomographic reconstruction calculation, giving the 3D distribution of structural constituents (Fig. 2a). In this data acquisition process, we assume that the sample structure is stable and exhibits little change. Although time-resolved microtomographic analysis has been achieved by acquiring a dataset within a few seconds [5], most microtomographs are designed to acquire a dataset by taking from a few minutes to several tens of minutes. Sample drift or deformation faster than the data acquisition process causes reconstruction artifacts in the resultant microtomogram. Therefore, all the constituents in the sample should be structurally fixed for the duration of the data acquisition. Because biological samples are mostly composed of soft tissues, they are usually embedded in epoxy resin [6] to fix their structures. We have already reported detailed protocols for preparing such microtomographic samples [7]. As a rule of thumb, resin embedding is essential for the visualization of 3D structures at a resolution of a few micrometers or finer.

2.2 Spatial resolution

In many microtomographic analysis cases, the pixel width of the 2D radiograph is set to around half the x-ray optics resolution to minimize the amount of raw data, which typically reaches over 1 Gbyte. This Nyquist criterion has also been applied to image sampling in clinical CTs [8,9]. However, the spatial resolution is the most important concern in microtomographic analysis. From the sampling theorem, a 2D image should be taken with a pixel width of less than $1/2\sqrt{2}$ times the spatial resolution [10]. This can be generalized by stating that an *N*-dimensional image should be digitized with a pixel width of less than $1/2\sqrt{N}$ times the spatial resolution. Therefore, radiograph sampling at half the spatial resolution is sufficient for microtomographic data acquisition but insufficient for reconstruction calculation. The 3D microtomographic image should be digitized with a pixel width of $1/2\sqrt{3}$ times the spatial resolution. This pixel width can be achieved by taking radiographs with a finer pixel width or by interpolating the radiographs with zoom reconstruction [11], which gives a pixel width of 1/2 or 1/4 of the acquired radiographs (Fig. 2b). We have implemented this zoom reconstruction method in the program RecView (available from http://www.el.u-tokai.ac.jp/ryuta/).

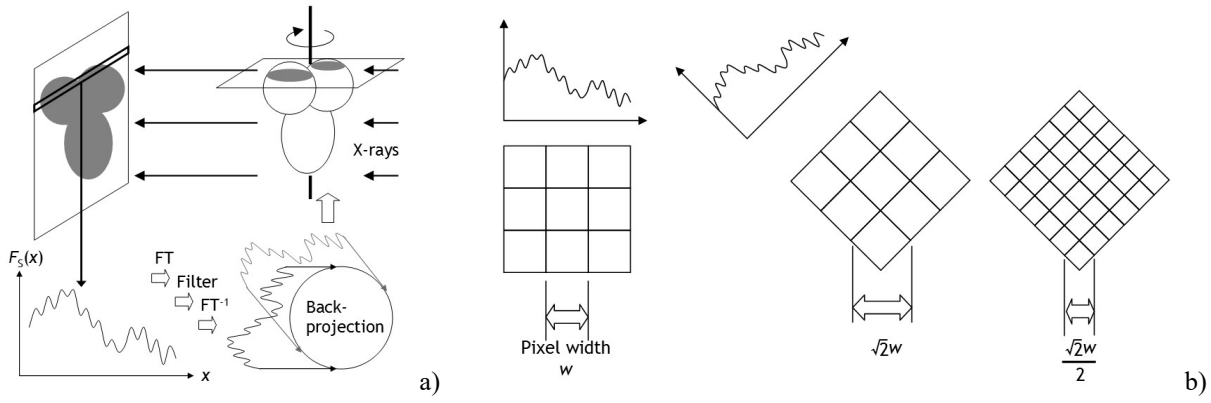

Fig. 2 (a) 2D radiographs are taken by rotating the sample. The horizontal pixel strip extracted from the 2D radiograph was subjected to Fourier transformation, application of a filter function, and inverse Fourier transformation. Back-projection calculations were then performed to obtain the microtomogram. (b) Radiographs taken with a pixel width *w* were back-projected with a broadened projection width of about 1.4*w* when the filtered strip was projected from an angle of 45°. The broadening can be avoided by applying zoom interpolation prior to the tomographic reconstruction.

The spatial resolution of the reconstructed microtomogram can be examined by using 3D micro test objects [11-13]. Spatial resolution in real space is usually estimated from the modulation transfer function (MTF) that describes the dependence of intensity reproducibility with respect to the structure's fineness. The microtomographic MTF is actually determined from the intensity profile of periodic patterns [11,12] or sample edges [13]. Although periodic patterns should be prepared by carving rectangular wells on the test object's surface, as seen in Figure 1, flat surfaces of crystals or edge structures found in the sample itself can be used for *in situ* MTF estimation. It is also necessary to note that the in-plane resolution within the tomographic slice is affected by the reconstruction calculation, while the through-plane resolution along the rotation axis is mainly independent of the tomographic reconstruction. Therefore, both the in-plane

and through-plane resolutions should be estimated separately. Examples of spatial resolutions of microtomographs available at the synchrotron radiation facility SPring-8 (Hyogo, Japan) are given in Table 1.

Table 1 Spatial resolutions of simple projection microtomographs at SPring-8.

Beamline	BL20B2	BL20XU, BL47XU
Number of projections per 180°	1800	1800
Pixel size (μm)	2.75	0.5
2D resolution (μm)	~8	1[b]
In-plane tomographic resolution[a] (μm)		
Square wave pattern	8.5[c]	0.8[d]
Edge response	-	0.9[e]
Through-plane resolution (μm)		
Square wave pattern	8.0[c]	0.8[d]

a) Tomographic resolutions were estimated at 5% MTF using the zoom reconstruction.
b) Resolution reported in ref. 14; c) in ref. 11; d) in ref. 12; e) in ref. 13.

There has been discussion that the resolution of simple projection optics in the synchrotron radiation microtomographs depends on the thickness of the fluorescence screen of the imaging detector [15]. Higher microtomographic resolution achieved with zone plate optics depends on the x-ray optics setup. Most laboratory microtomographs are equipped with microfocus x-ray generators whose focal size determines the spatial resolution.

2.3 Viewing field

Viewing field sizes are another important concern in tomographic visualization. The dimensions of the tomographic slice plane are determined by the pixel width and number of pixels along the direction perpendicular to the sample rotation axis. If we choose the rotation axis to be along the vertical direction in a parallel-beam geometry, then a radiograph with 2000 horizontal pixels with an effective pixel size of 0.5 μm is reconstructed into a 2000 x 2000 pixel tomogram corresponding to a tomographic viewing field of 1.0 mm in diameter. Naturally, the sample should be illuminated with x-rays all over the detector area. The dimension perpendicular to the tomographic slice is determined by the number of pixels along the rotation axis. In the above example, the 3D viewing field reconstructed from a radiograph with 2000 horizontal and 1000 vertical pixels covers 1.0 mm in diameter x 0.5 mm in height.

In tomographic analysis, we assume that the sample cross-section is accommodated in the tomographic viewing field in the slice plane. If the sample leaves this viewing field, image intensities around the viewing field boundaries are disturbed in the reconstruction calculation, though the image shape is not severely deteriorated. Therefore, even when the outside dimension of the sample cannot be fitted within the tomographic viewing field, the structure of the region of interest can be visualized by microtomography if the local shape of the region of interest rather than the image intensity should be determined.

As described in the following section, 2D radiographs in the range from 0° to 180° should be acquired for tomographic reconstruction. The obtained dataset contains all the possible projection images of the sample rotated around the defined axis. This data acquisition is usually performed by placing the rotation axis at the center of the detector viewing field. Another strategy for acquiring a dataset is to take radiographs by placing the axis near the left or right end of the viewing field. For example, if the rotation axis is placed near the right end, the left half of the sample image is taken at 0° and the right half at 180°. Therefore, the whole dataset can be taken by rotating the sample from 0° to 360°. This data acquisition method is known as offset CT; it is used to double the width of the viewing field.

In contrast to the viewing field width, there is no need to arrange the sample to be accommodated within the viewing field height along the rotation axis. This height dimension of the viewing field can be extended by scanning the sample along the rotation axis and stacking the obtained microtomograms [16].

2.4 Data acquisition

Once the required spatial resolution and viewing field have been defined, data acquisition parameters can be configured. The important parameters for the tomographic data acquisition are rotation angle and exposure time per radiograph frame.

2D radiographs from every direction should be taken in order to reconstruct the 3D image. This is accomplished by taking radiographs while rotating the sample from 0° to 180° in the normal CT setup or from 0° to 360° in the offset CT setup. Because the tomographic reconstruction is usually performed by the back-projection method (Fig. 2a), each radiograph should be taken with a fine step of $R\Delta\theta$ in the circumferential direction, where R denotes the distance from the rotation axis and $\Delta\theta$ the rotation angle per frame. For example, if the detector width is 2000 pixels and the rotation axis is placed at the center, the maximum distance R from the axis is 1000 pixels. Each pixel in the reconstructed tomogram can be resolved by taking an $R\Delta\theta$ step of less than 1. Therefore, the rotation angle per frame $\Delta\theta$ should be

less than 0.001 radians or 0.0572° to resolve the outer circumferential pixels in the tomogram. If $\Delta\theta$ is set to 0.05°, a total of 3600 frames from 0° to 180° should be acquired to determine one 3D image. Because long data acquisition increases the possibility of sample drift, leading to reconstruction artifacts in tomograms, the $\Delta\theta$ step is sometimes set to 0.10°, corresponding to 1800 frames from 0° to 180°.

In the tomographic reconstruction calculation, it is assumed that the incident x-rays are not completely absorbed by the sample. Therefore, the exposure time should be long enough to detect the transmitted x-rays. However, individual pixels in the detector should not be overloaded beyond their dynamic range. The exposure time is determined from these criteria, *i.e.,* the pixel values should be sufficiently larger than dark current and smaller than the detection maximum. In the most typical setup in our experiment, we took radiographs for 200–1000 ms per frame with a 12-bit dynamic range detector using monochromated synchrotron radiation.

The signal observed over N times is built up to an N-fold intensity, whereas the normally distributed noise is $\sqrt{N}$-fold. The resultant signal-to-noise ratio is given by $N/\sqrt{N} = \sqrt{N}$. This indicates that a longer exposure will improve the image quality of tomograms. However, as discussed above, the pixel intensity should be within the detector dynamic range and should not be overloaded. In order to improve the signal-to-noise ratio, besides the exposure time per frame, the number of frames should be increased by taking a finer $\Delta\theta$ step to increase the total exposure. In the example shown in Figure 3, 1800 frames with a 0.1° step and 350-ms exposure gave an exposure time of 630 s, while 4500 frames with a 0.04° step and 1000-ms exposure gave an exposure time of 4500 s, corresponding to an approximately 2.7-fold improvement in the signal-to-noise ratio.

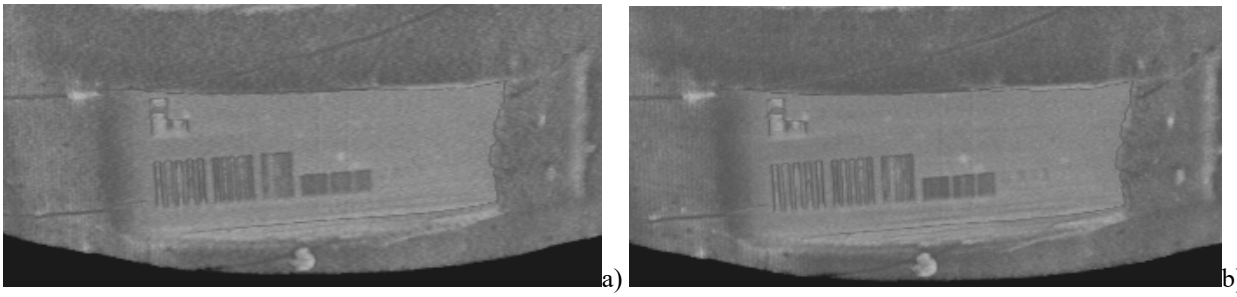
a) b)

Fig. 3 Microtomographic images of a test object reconstructed from radiographs where the total exposure was 630 s (a) or 4500 s (b). Although the object's surface looks noisy in panel (a), the same surface exhibits a rather precise profile with a longer exposure (b).

3. X-ray visualization of biological structures

Biological tissues are mainly composed of light elements, which produce little contrast in x-ray images. One of the methods of visualizing structures with poor absorption contrast is phase contrast imaging. The phases of x-ray waves that pass through any material are affected by the electron density distribution in the material. The microstructure of lung alveoli has been visualized with refraction enhancement imaging [17], which is the same in principle as phase contrast imaging. In this case, we can interpret structures with high electron density as alveolar walls and those with low density as air. However, it is not always true that biological structures can be interpreted from the electron density distribution. The electron densities of most biological constituents have no inherent relationship with their biological functions.

In clinical diagnosis, the luminal structures of a living body are visualized by using x-ray contrast media. These contrast media contain high-Z elements, such as iodine or barium, those absorb hard x-rays efficiently. Therefore, x-ray visualization of the microstructures of soft tissues can be performed by specifically contrasting each biological constituent with a high-Z element probe, which corresponds to the fluorescent label in light microscopy. Probe elements that have been reported for contrasting biological microstructures include gold [6,18-20], platinum [19,20], silver [16], osmium [7, 21-24], and iodine [25,26]. Most of these elements are in the fifth or sixth row of the periodic table because the high-Z elements exhibit high electron densities that can give sufficient x-ray contrast.

Each element has specific x-ray absorption edges corresponding to the energy levels of electron orbitals. The x-ray absorption spectra of the metals platinum and gold are shown in Figure 4a. The horizontal axis represents x-ray energy E, which is the reciprocal of the x-ray wavelength λ, where E (keV) = 12.398/λ (Å). For synchrotron radiation microtomographs, radiation from the storage ring is usually monochromated to obtain x-rays with a certain energy. The available energy and brilliance of the monochromated beam depend on the radiation source, monochromator, and other beamline components. The radiation from bending magnets or insertion devices at third-generation synchrotron radiation facilities ranges from infrared light to hard x-rays, though we use x-rays of 8 keV to 15 keV for imaging biological samples because soft tissue is almost transparent in this range and stained structures are clearly visualized with appropriate contrast. To maximize the image contrast, the x-ray energy at the top of the absorption edge of the probe element should be used. For example, x-ray energy of 12 keV corresponding to the top of the Au L_{III} edge should

be chosen to visualize structures stained with gold. The tomographic reconstruction is performed by taking into account the monochromatic x-ray transmittance at each pixel in the 2D radiograph and the voxel size of the resultant 3D image. Therefore, the voxel values of the obtained tomograms are calculated as a linear absorption coefficient at the observed x-ray energy. These observed absorption coefficients can be calibrated with standard materials. Element-specific visualization can be performed by subtracting the x-ray intensities at the bottom of the absorption edge from those at the edge top. The distributions of multiple high-Z probes can be individually visualized by using the x-ray absorption edge of each probe element [19], as shown in Figure 4b.

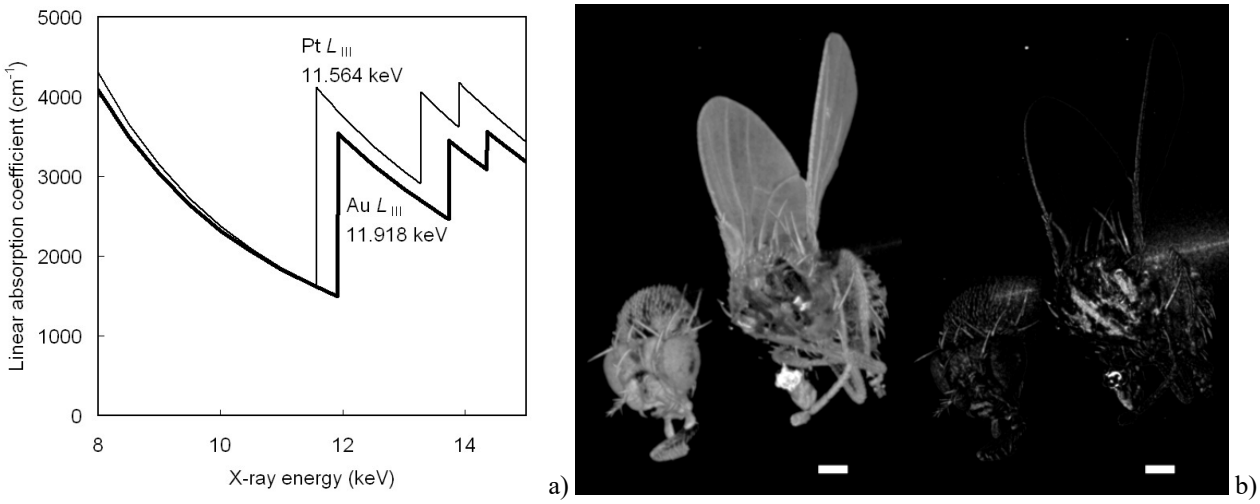

Fig. 4 (a) X-ray absorption spectrum of platinum is represented by the thin line and that of gold by the bold line. L_{III} edges are indicated with edge energies. (b) Adult *Drosophila* fruit fly structures analyzed at Au L_{III} (left) and Pt L_{III} absorption edges (right) [19]. The gold image indicates that every constituent was visualized, whereas the platinum image gives a specific distribution of the platinum compound administrated as a feed ingredient. The gold image was produced by subtracting the 3D distribution of linear absorption coefficients at 11.910 keV from that at 11.930 keV. The platinum image was produced by subtracting the 11.550-keV image from the 11.570-keV image. The abdominal region was severed to reveal the visceral structure in the 3D images. CT densities are rendered at difference linear absorption coefficients of +1.2 cm^{-1}. Scale bar: 200 μm.

For laboratory microtomographs, the operating voltage and target material of the microfocus x-ray generator determine the x-ray spectrum. Because the microfocus generators are usually used without a monochromator, the spectrum of incident x-rays is regarded as superposition of white x-rays with a broad profile and characteristic x-rays with sharp peaks. The x-ray energy of the characteristic x-rays depends on the target material (*e.g.*, Cu*K*α radiation of 8.041 keV for a copper target), while that of white x-rays depends on the operating voltage. A sample image taken with the laboratory microtomograph is, therefore, given as an overall transmittance of the white and characteristic x-rays. The high-energy component of the x-ray spectrum can readily pass through sample, while the low-energy x-rays are effectively absorbed by the sample. This truncation in the energy profile of the transmitted x-rays is known as beam hardening and should be considered when microtomograms are taken using a generator source. For this reason, the voxel density of 3D images visualized using the laboratory microtomographs does not represent the x-ray absorption coefficient.

We have reported a radiographic visualization of neural tissue at 160-nm resolution [6] by using x-ray optics with a Fresnel zone plate. The application of zone plate optics to microtomographic analysis enables the visualization of nanometer-scale structures such as synapses and membrane rafts. The nanometer-scale image should be digitized with an effective pixel size of the nanometer order. Although x-ray condenser optics can be used to increase the number of incident photons, the nanometer-scale analysis results in fewer x-ray photons per detector pixel. Therefore, phase contrast imaging should facilitate the visualization of nanometer-scale structures even when the structure contrast is enhanced by high-Z element staining.

4. Interpretation of biological microstructures

Although microtomographic analysis has entered general usage with recent progress in x-ray optics and x-ray microscopy, the scientific understanding of 3D microtomographic images is still advancing. This is mainly due to the complexity of the 3D structures visualized by microtomography. If a methodology for handling the 3D distribution of x-ray absorption coefficients is established, information embedded in the 3D structure can be analytically elicited.

We have recently reported microtomographic visualization of 3D neuronal structures of human cerebral cortex [27]. Neuronal circuits are built up by neurons as 3D networks. Therefore, unveiling the 3D neuronal structures is the first step in understanding the mechanism of brain functions. However, the 3D structure of brain tissue is much too

complicated to enable analytical resolution of the neuronal circuits. The 3D rendering of mouse brain tissue in Figure 5 indicates that cell layers and the accompanying network structures were visualized, but their neuronal circuits cannot be resolved by just visualizing the 3D structure.

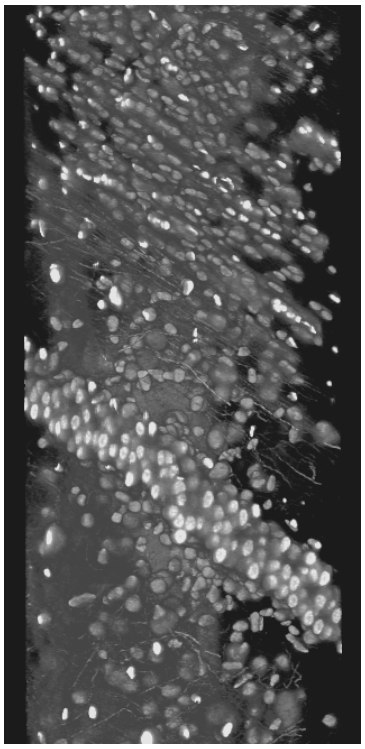

Fig. 5 3D rendering of microtomographic structure of mouse brain tissue. Neural cell layers and neuropil networks were visualized as 3D distribution of linear absorption coefficients. Densities were rendered from the coefficient of 23.5 cm^{-1} (black) to 51.5 cm^{-1} (white) by the scatter HQ algorithm using the program VG Studio MAX (Volume Graphics, Germany).

Similar complicated 3D structures of biological macromolecules of proteins and nucleic acids have been determined by crystallographic analysis. In macromolecular x-ray crystallography, the 3D distribution of electron density is traced to build an atomic model of the target molecule (Fig. 6a). The model is composed of a large number of 3D Cartesian coordinates of the atoms. Although it is practically impossible to comprehend the electron density map itself, the skeletonized atomic model built in the electron density map allows us to understand and discuss the biological functions of the target molecule on the basis of the structure.

We have applied this method to model building for 3D coefficient maps of human cerebral cortex visualized by microtomography [27]. The structure determination scheme is illustrated in Figure 6b by analogy to the method used in crystallography. First, the neuronal networks and capillary vessel architectures in the cerebral cortex tissue were visualized as a 3D distribution of x-ray absorption coefficients. Skeletonized wire models of the structural constituents were built by placing and connecting nodes in the 3D coefficient map. The model-building procedures were similar to those reported for crystallographic analyses of macromolecular structures, while neuronal networks were automatically traced by using a 3D Sobel filter. The cell types of the models were determined from the morphology of somata and dendrites. The 3D structure of the obtained models clarified the network structures embedded in the brain tissue. The neuronal circuits were then analytically resolved from the skeletonized models. This analytical approach based on the 3D structure of the neuronal networks allows discussion of the operating mechanism of the neuronal circuits in the human brain [27].

Simplification of the 3D density distribution by building skeletonized models in absorption coefficient maps facilitates understanding of the 3D structures of biological objects. The models built in the brain tissue can be used to unveil the functional mechanism of the brain. Any fibrous network structures can be traced and analyzed by using a similar method. Aggregated structures could be modeled by dividing them into small elements, which could be used for computational simulation. We suggest that x-ray microtomography along with model building in the 3D coefficient map is a potential method for understanding 3D microstructures relevant to biological functions, like x-ray crystallography in molecular biology.

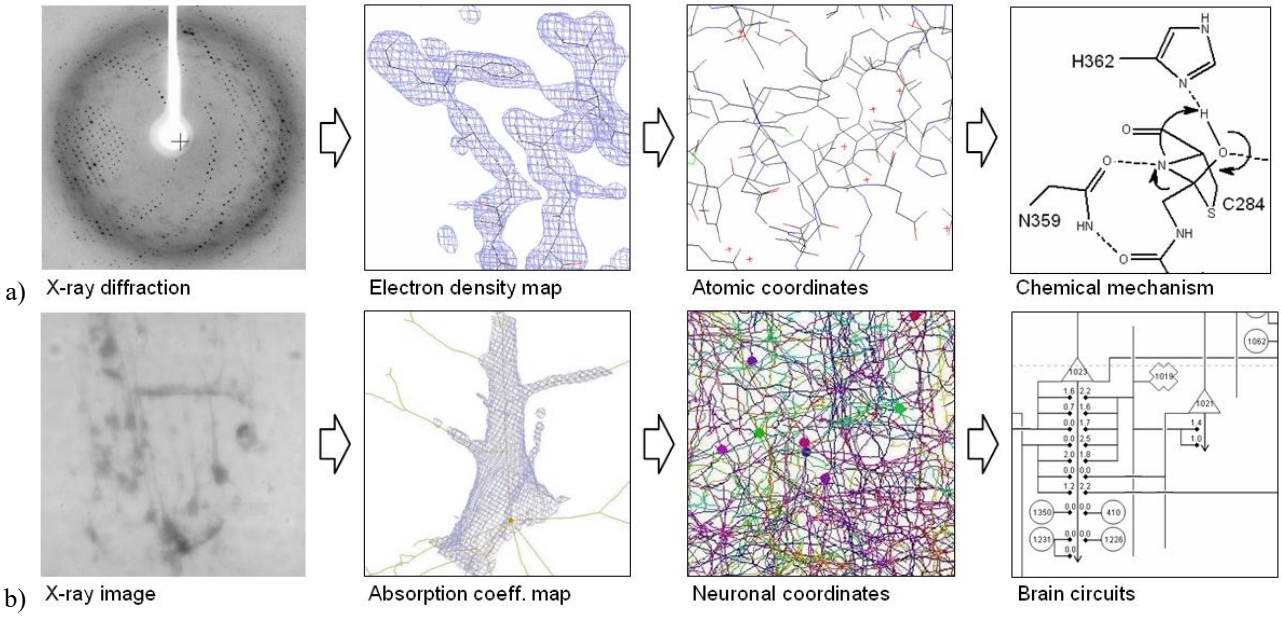

Fig. 6 (a) In crystallographic structure determination, observed diffraction amplitudes along with separately estimated diffraction phases are subjected to Fourier transformation, giving electron density maps. Atomic coordinates are then determined by placing atoms of the target molecule on the map. The resultant model can be used for discussing the chemical mechanisms or molecular interaction of the target. These figures are given as examples from the crystallographic analysis of a DNA endonuclease [28]. (b) In microtomographic structure determination, observed x-ray images are subjected to the tomographic reconstruction calculation, giving 3D maps of x-ray absorption coefficient or electron density. Cellular and subcellular structures are modeled by placing and connecting nodes on the map. The resultant model can be used to resolve the functional principle of the target, such as brain circuits composed of neurons. These figures are taken from the microtomographic analysis of human cerebral cortex [27].

Acknowledgments We thank Dr. J. Matsuda, Institute of Glycoscience, Tokai University, for discussion about the mouse anatomy. We thank R. Takei and M. Kanno, School of Engineering, Tokai University, for helpful assistance with sample preparation and microtomographic analysis. We also thank Y. Miyamoto, Technical Service Coordination Office, Tokai University, for focused ion-beam milling. This study was supported in part by Grants-in-Aid for Scientific Research from the Japan Society for the Promotion of Science (no. 21611009). The synchrotron radiation experiments were performed at SPring-8 with the approval of the Japan Synchrotron Radiation Research Institute (JASRI) (proposal nos. 2000A0356, 2000A0486, 2001A0241, 2006A1191, 2006B1716, 2007A1844, 2007A2072, 2007B1102, 2007B1894, 2008A1190, 2008B1261, 2009A1113, and 2009B1191).

References

[1] Conchello J-A, Lichtman JW. Optical sectioning microscopy. *Nat. Methods.* 2005;2:920-931.
[2] Bonse U, Busch F. X-ray computed microtomography (microCT) using synchrotron radiation (SR). *Prog. Biophys. Mol. Biol.* 1996;65:133-169.
[3] Salomé M, Peyrin F, Cloetens P, Odet C, Laval-Jeantet AM, Baruchel J, Spanne P. A synchrotron radiation microtomography system for the analysis of trabecular bone samples. *Med. Phys.* 1999;26:2194-2204.
[4] Uesugi K, Tsuchiyama A, Nakano T, Suzuki Y, Yagi N, Umetani K, Kohmura Y. Development of microtomography imaging system for rock and mineral samples. *Proc. SPIE.* 1999;3772:214-221.
[5] Di Michiel M, Merino JM, Fernandez-Carreiras D, Buslaps T, Honkimäki V, Falus P, Martins T, Svensson O. Fast microtomography using high energy synchrotron radiation. *Rev. Sci. Instrum.* 2005;76:043702.
[6] Mizutani R, Takeuchi A, Hara T, Uesugi K, Suzuki Y. Computed tomography imaging of the neuronal structure of Drosophila brain. *J. Synchrotron Radiat.* 2007;14:282-287.
[7] Mizutani R, Takeuchi A, Uesugi K, Takekoshi S, Osamura RY, Suzuki Y. Three-dimensional microstructural analysis of human brain tissue by using synchrotron radiation microtomographs. In: Westland TB, Calton RN, eds. *Handbook on White Matter*. New York, NY: Nova Science Publishers; 2009:247-277.
[8] Lin PJP. *et al*. *AAPM Report No. 39: Specification and Acceptance Testing of Computed Tomography Scanners*. New York, NY: American Institute of Physics; 1993.
[9] Goldman LW. Principles of CT: radiation dose and image quality. *J. Nucl. Med. Technol.* 2007;35:213-225.
[10] Pawley JB. Points, pixels, and gray levels: digitizing image data. In: Pawley JB, ed. *Handbook of Biological Confocal Microscopy* third ed. New York, NY: Springer Science+Business Media; 2006:59-79.
[11] Mizutani R, Takeuchi A, Uesugi K, Suzuki Y. Evaluation of the improved three-dimensional resolution of a synchrotron radiation computed tomograph using a micro-fabricated test pattern. *J. Synchrotron Radiat.* 2008;15:648-654.

[12] Mizutani R, Takeuchi A, Osamura RY, Takekoshi S, Uesugi K, Suzuki Y. Submicrometer tomographic resolution examined using a micro-fabricated test object. *Micron.* 2010;41:90-95.
[13] Mizutani R, Taguchi K, Takeuchi A, Uesugi K, Suzuki Y. Estimation of presampling modulation transfer function in synchrotron radiation microtomography. *Nucl. Instrum. Meth. A*. 2010; 621:615-619.
[14] Uesugi K, Suzuki Y, Yagi N, Tsuchiyama A, Nakano T. Development of high spatial resolution X-ray CT system at BL47XU in SPring-8. *Nucl. Instrum. Meth. A.* 2001;467-468:853-856.
[15] Uesugi K, Takeuchi A, Suzuki Y. High-definition high-throughput micro-tomography at SPring-8. *J. Physics Conf. Ser.* 2009;186:012050.
[16] Mizutani R, Takeuchi A, Uesugi K, Ohyama M, Takekoshi S, Osamura RY, Suzuki Y. Three-dimensional microtomographic imaging of human brain cortex. *Brain Res.* 2008;1199:53-61.
[17] Suzuki Y, Yagi N, Uesugi K. X-ray refraction-enhanced imaging and a method for phase retrieval for a simple object. *J. Synchrotron Radiat.* 2002;9:160-165.
[18] Mizutani R, Hara T, Takeuchi A, Uesugi K, Suzuki Y. Microtomographic analysis of Drosophila brain. *Biophysics* (*The Fifth East Asian Biophysics Symposium*: The Biophysical Society of Japan). 2006; 46:S388.
[19] Mizutani R, Takeuchi A, Uesugi K, Takekoshi S, Osamura RY, Suzuki Y. X-ray microtomogaphic imaging of three-dimensional structure of soft tissues. *Tissue Eng. Part C*. 2008;14:359-363.
[20] Mizutani R, Takeuchi A, Akamatsu G, Uesugi K, Suzuki Y. Element-specific microtomographic imaging of Drosophila brain stained with high-Z probes. *J. Synchrotron Radiat.* 2008;15:374-377.
[21] Johnson JT, Hansen MS, Wu I, Healy LJ, Johnson CR, Jones GM, Capecchi MR, Keller C. Virtual histology of transgenic mouse embryos for high-throughput phenotyping. *PLoS Genet.* 2006;2:e61.
[22] Litzlbauer HD, Neuhaeuser C, Moell A, Greschus S, Breithecker A, Franke FE, Kummer W, Rau WS. Three-dimensional imaging and morphometric analysis of alveolar tissue from microfocal X-ray-computed tomography. *Am. J. Physiol. Lung Cell. Mol. Physiol.* 2006;291:L535-L545.
[23] Ananda S, Marsden V, Vekemans K, Korkmaz E, Tsafnat N, Soon L, Jones A, Braet F. The visualization of hepatic vasculature by X-ray micro-computed tomography. *J. Electron Microsc*. 2006;55:151-155.
[24] Lareida A, Beckmann F, Schrott-Fischer A, Glueckert R, Freysinger W, Müller B. High-resolution X-ray tomography of the human inner ear: synchrotron radiation-based study of nerve fibre bundles, membranes and ganglion cells. *J. Microsc.* 2009;234:95-102.
[25] de Crespigny A, Bou-Reslan H, Nishimura MC, Phillips H, Carano RA, D'Arceuil HE. 3D micro-CT imaging of the postmortem brain. *J. Neurosci. Methods*. 2008;171:207-213.
[26] Metscher BD. MicroCT for comparative morphology: simple staining methods allow high-contrast 3D imaging of diverse non-mineralized animal tissues. *BMC Physiol*. 2009;9:11.
[27] Mizutani R, Takeuchi A, Uesugi K, Takekoshi S, Osamura RY, Suzuki Y. Microtomographic analysis of neuronal circuits of human brain. *Cereb. Cortex*. 2010; 20: 1739-1748.
[28] Mizutani R, Nogami S, Kawasaki M, Ohya Y, Anraku Y, Satow Y. Protein-splicing via a thiazolidine intermediate: crystal structure of the VMA1-derived endonuclease bearing the N- and C-terminal propeptides. *J. Mol. Biol.* 2002;316:919-929.